UPDATE ON SOLEIL II BOOSTER

V. Kubytskyi*, P. Alexandre, E. Kravishvili, A. Loulergue, M.-A. Tordeux,
Synchrotron SOLEIL, Saint-Aubin, France

Abstract

SOLEIL II is a synchrotron light source aiming to deliver extremely high-brightness beams in the soft-tender X-ray range [1]. The storage ring will operate with an electron beam emittance below 100 pm·rad. To ensure efficient injection into the storage ring, the emittance of the electron beam extracted from the booster must be in the few-nm·rad range (5.2 nm·rad compared to 140 nm·rad for the present booster). To achieve these beam parameters, the booster injection energy is increased from 110 MeV to 150 MeV, and a new booster with a modified 16BA lattice has been designed [2, 3]. We show that the booster design has now converged towards its final configuration: the main dipoles of the 14BA arcs and 2BA matching sections are defined, the booster circumference is fixed, and the beam dynamics along the energy ramp has been studied including both systematic and random multipolar components.

INTRODUCTION

We report on the recent progress and studies for the new Booster of the SOLEIL II project. A completely new booster will be constructed, with a low natural beam emittance of 5.2 nm rad at the extraction energy of 2.75 GeV, compared with 140 nm rad delivered by the present booster. The new booster will occupy the location of the current booster, keeping the racetrack geometry and requiring only minor adaptations to the injection and extraction geometry. Booster operation should remain stable and reliable. The increase of the injection energy to 150 MeV is favourable for the new booster in terms of stability and injection efficiency, remanent fields in booster magnets, reduction of geometrical emittance, sensitivity to linac jitter, beam-gas lifetime and space-charge effects. We use two existing acceleration sections, for the linac energy upgrade which will be performed summer 2026. Injection into the present booster and operation at 150 MeV will take place once authorisation from the French Nuclear Safety Authority is received. The main parameters of the new booster are given in Table 1.

The booster lattice is based on a 16BA higher-order achromat superperiod, composed of 14BA optics in the arcs and 2BA optics in the matching sections. The arc unit cell, shown in Fig. 1, consists of a defocusing dipole D2, two defocusing sextupoles, two focusing quadrupoles and one focusing sextupole. The lattice design was discussed in detail in Ref. [2].

The procurement of assembled girders, including measured and aligned magnets, UHV-clean vacuum chambers and BPMs, is planned for 2027. The booster arc design is being developed toward an integrated implementation of magnets, supports, vacuum chambers and diagnostics.

* viacheslav.kubytskyi@synchrotron-soleil.fr

Table 1: Booster Main Parameters

Parameter	Unit	Present booster	Upgrade booster
Energy range	GeV	0.11–2.75	0.15–2.75
Circumference	m	156.6	156.569
Natural emittance	nm rad	140	5.2
Betatron tunes (H/V)	–	6.65/4.58	13.18/4.195
Natural chromaticities	–	−7.3/ − 5.8	−27/ − 12
Momentum compaction factor	–	2.8×10^{-2}	3.3×10^{-3}
Damping partitions	–	1.0/1.0/2.0	1.6/1.0/1.4
Natural damping times	ms	6.3/5.7/2.7	3.3/5.2/3.7
Energy loss per turn	keV	409	554
Natural energy spread	–	0.66×10^{-3}	0.93×10^{-3}
RMS bunch length	ps	50 at 3.6 MV	25 at 3 MV

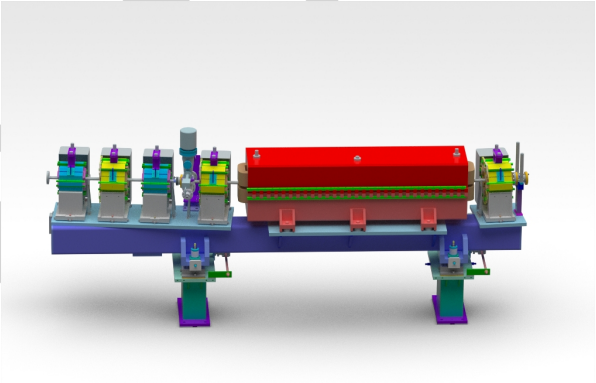

Figure 1: Arc girder with magnetic elements placed.

Several items of equipment have been identified as reusable or adaptable for the new booster: RF cavities, DCCT/FCT, striplines for tune measurement, beam-position screens, injection pulsed magnets and quadrupole power supplies. Some of this equipment belongs to the present storage ring. This strategy reduces the total cost of the booster upgrade while keeping well-known and reliable equipment.

In terms of booster diagnostics, eight BPMs are located in the straight matching sections, and each arc unit cell is equipped with a BPM situated at the end of the girder. This design choice facilitates the installation and alignment of the girders. A dedicated study was performed to optimise the girder placement in terms of orbit-correction performance. The robustness of the booster lattice design with respect to realistic misalignments and calibration errors was presented in detail in Ref. [3].

BOOSTER CIRCUMFERENCE

Prior to booster construction and the placement of the lattice elements in the 3D layout, the circumference must be known accurately. The booster circumference is defined consistently with the storage ring, since both machines share the same master clock. The booster circumference is therefore fixed by the exact ratio of the harmonic numbers, 184 for the booster and 416 for the storage ring, as in the present SOLEIL injector. When the booster is ramped from 150 MeV to 2.75 GeV, the time of flight per turn is slightly longer at low energy. The booster circumference is optimised at injection energy, which is preferred in terms of optics and dynamic aperture in order to maximise the injection efficiency. Consequently, the booster must be shortened to restore the 184th harmonic at low energy for an on-momentum beam. At extraction energy, the reference orbit is then slightly off-momentum (+0.2%).

Another factor influencing the booster circumference is that the trajectory in the real magnetic field slightly differs from the hard-edge model due to the fringe fields. As for any dipole, the actual electron trajectory is shorter than the arc representing the dipole in the lattice model, due to the presence of leakage fields upstream and downstream of the magnet. This shortening must therefore be compensated for by lengthening the booster to maintain the 184th harmonic. To accurately evaluate the realistic trajectory length, we performed tracking in the 3D dipole field maps with RF-Track [4]. We demonstrate it on the example of combined function magnet D2 defocusing dipole (Fig. 2), which is present in each unit cell of arc, in total 28 such magnets. The design of D2 dipole required for the new booster is the result of the optimisation of poles geometry with requirements for bending angle, magnetic length, gradient and multipolar components. We use obtained 3D fieldmaps (Opera3d software) in our RF-Track simulation.

Accurate tracking in the fieldmap requires few preparatory steps. The equivalent magnetic length and bending angle of the magnet is first calculated by particle tracking starting from the center of the field map. From these parameters, we define symmetrical entry and exit points in a region where there is no residual magnetic field. These points also correspond to the entry/exit points of the equivalent hard-edge magnet, supplemented by drifts on either side. The center of the actual dipole is the center of the field map (0,0), while the center of the hard-edge magnet is offset by δh. With tracking at 2.75 GeV, we verify that the trajectory is symmetrical, passes through (0,0), and coincides with the trajectory generated by the Opera software. We then evaluate the length of this trajectory and compare it to that of the hard-edge model, known by construction: Arc + 2 × Drift. The difference gives us the shortening of the path length in the realistic dipole. Tracking the full ring with field maps in RF-Track gives the same fractional tunes as the AT lattice with sliced dipoles. Trajectory shortening and the corresponding offset of the magnet centres for both dipole types, D1 and D2, are summarised in Table 2

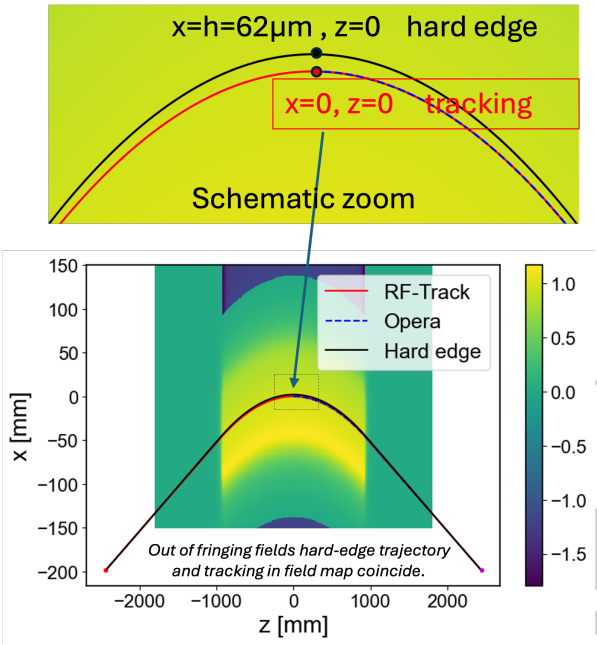

Figure 2: Trajectory in dipole D2 and comparison with the hard-edge model.

Table 2: Dipole Contribution to Path Length Shortening

Dipole	Transverse offset h [mm]	Path length shortening [mm]
Single D1	–0.100	–0.016
Single D2	–0.062	–0.012
4 D1 + 28 D2	–	–0.404

Therefore, at the injection energy of 150 MeV, the nominal circumference, including the time-of-flight correction and the trajectory shortening in the dipoles, is evaluated as $C_{\text{ideal}} - 0.9\,\text{mm} + 0.4\,\text{mm} = 156.569\,\text{m}$, where $C_{\text{ideal}} = 184c/f_{\text{RF,SR}}$, with $f_{\text{RF,SR}} = 352.314252e6$ Hz.

The booster will be constructed according to this nominal circumference specification. Table 3 gives the alignment and frequency-stability requirements. A change of the booster circumference can be expressed through the following equivalent variations: $\Delta C = +1$ mm for the storage-ring circumference, $\Delta C = +0.44$ mm for the booster circumference, $\Delta f_{\text{RF}} = -1$ kHz for the RF frequency variation, $\Delta E/E = +10^{-3}$ for the relative energy offset of the booster beam, and $\Delta T = +0.33$ °C for a uniformly distributed temperature change in the booster tunnel.

ENERGY RAMPING PROCESS

The D2 dipoles will be powered by four power supplies, whereas the other magnets are powered by one power supply per family. We studied the effect of tracking errors along the ramp and compared possible cabling schemes for the arc dipoles. A constant relative tracking error of 5×10^{-4} was assigned to each power supply, and 30 random seeds

Table 3: Alignment and Frequency Stability Requirements

Parameter	Max Value
Spec. for circumference alignment of the Storage Ring	±2 mm
Spec. for circumference alignment of the Booster	±2 mm
Spec. of Booster tunnel temperature	±1°
Sustainable frequency drift over years of operation, before any realignment of the Booster	3 kHz

were studied for each configuration are shown in Fig. 3. The optimal pattern, which generates the smallest orbit excitation, is the sequential cabling pattern 1–2–3–4–1–2–3–4. This can be explained by the homogeneous distribution of errors around the ring and by local averaging between neighbouring power supplies. In contrast, patterns with a long spatial period are less favourable because they can drive coherent orbit excitations requiring stronger correctors.

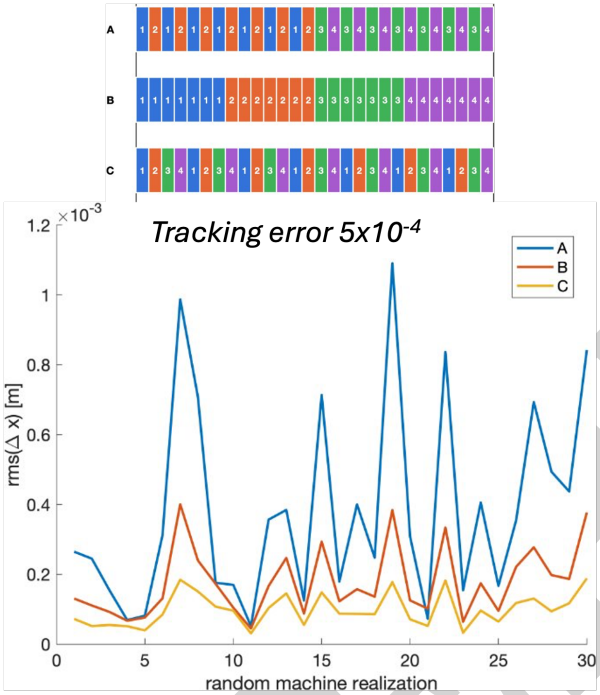

Figure 3: Effect of the cabling pattern of the four D2-dipole power supplies on the residual orbit in the presence of tracking errors.

We performed turn-by-turn tracking along the ramp using the fast-ring method of AT [5]. The ring is represented by a one-turn 6D transfer matrix, a quantum-diffusion element and RF cavity element. The fast-ring model is used to track a beam of 10000 particles generated according to the injected beam emittance. To reduce the simulation time while staying within the AT framework, the fast-ring physics model is updated at fixed energy intervals of 1 MeV. At each energy step, the optics map, radiation-damping coefficients and quantum-diffusion terms are refreshed. During the step, the fast-ring model is kept fixed, while the particle coordinates are updated every turn to the new reference momentum. Radiation damping and quantum diffusion act every turn, but their coefficients are not recomputed at every turn. This allows us to significantly speed up the booster ramp simulation, keeping the lattice parameters close to realistic ones, and include, for example, the effect of induced sextupolar components in the beampipe due to eddy currents.

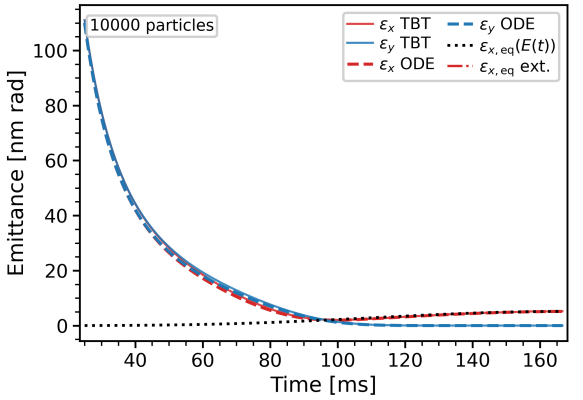

Figure 4: Evolution of the horizontal and vertical emittances during the energy ramp. Turn-by-turn tracking results are compared with the ODE model and with the instantaneous equilibrium horizontal emittance computed along the ramp.

Figure 4 shows that the large injected emittance is rapidly damped during the first part of the ramp. The turn-by-turn tracking agrees closely with the prediction of the numerically integrated emittance rate equations (ODE), which validates our fast-ring modelling study with radiation damping and quantum excitation during the ramp. At high energy, where the radiation damping time becomes short compared to the ramp duration, the horizontal emittance closely tracks the instantaneous equilibrium value $\varepsilon_{x,\mathrm{eq}}(E)$.

SUMMARY

The new SOLEIL II booster design has converged to a 16BA higher-order achromat lattice compatible with the existing injector geometry and the storage-ring RF constraints. The circumference budget was refined by including both the low-energy time-of-flight correction and the path-length shortening produced by realistic dipole fringe fields. Tracking in 3D dipole field maps with RF-Track confirms the consistency of the realistic dipole model with the sliced AT lattice.

The ramp studies show that the proposed fast-ring AT approach provides an efficient method to follow the emittance evolution turn by turn during the full energy ramp.

REFERENCES

[1] L. Nadolski *et al.*, "SOLEIL II: the French 4GLS Project – First Year of the Construction Program", presented at IPAC'26, Deauville, France, May 2026, paper TUO2M01, this conference.

[2] M.-A. Tordeux, A. Loulergue, R. Nagaoka, Z. H. Bai, T. Zhang, and G. Liu, "A low-emittance booster lattice design for the

SOLEIL upgrade", in *Proc. IPAC'21*, Campinas, Brazil, May 2021, pp. 410–413. doi:10.18429/JACoW-IPAC2021-MOPAB113

[3] P. Schreiber, F. Bouvet, M.-A. Tordeux, P. Alexandre, R. Ben El Fekih, S. Ducourtieux, and Z. Bai, "SOLEIL II booster robustness and emittance exchange", in *Proc. IPAC'24*, Nashville, TN, USA, May 2024, pp. 3071–3074. doi:10.18429/JACoW-IPAC2024-THPC36

[4] A. Latina, "The tracking code RF-Track and its application", in *Proc. HB'23*, Geneva, Switzerland, Oct. 2023, pp. 245–248. doi:10.18429/JACoW-HB2023-WEA3C1

[5] S. White, L. Carver, L. Farvacque, and S. Liuzzo, "Status and recent developments of Python Accelerator Toolbox", in *Proc. IPAC'23*, Venice, Italy, Sep. 2023, pp. 3185–3188. doi:10.18429/JACoW-IPAC2023-WEPL031